

1 **MUSCLEMOTION: a versatile open software tool to quantify**
2 **cardiomyocyte and cardiac muscle contraction *in vitro* and *in vivo***

3
4 Sala L., PhD^{#1}, van Meer B.J., MSc^{#1}, Tertoolen L.G.J., PhD¹, Bakkers J., PhD³, Bellin
5 M., PhD¹, Davis R.P., PhD¹, Denning C., PhD⁴, Dieben M.A.E., M.D.¹, Eschenhagen T.,
6 PhD⁵, Giacomelli E., MSc¹, Grandela C., PhD¹, Hansen A., PhD⁵, Holman E.R., M.D.⁶,
7 Jongbloed M.R.M., M.D., PhD^{1,6}, Kamel S.M., MSc³, Koopman C.D., MSc³, Lachaud Q.,
8 MSc², Mannhardt I., PhD⁵, Mol M.P.H., BSc¹, [Mosqueira D., MSc⁴](#) Orlova V.V., PhD¹,
9 Passier R., PhD^{1,7}, Ribeiro M.C., PhD⁷, Saleem U., PhD⁵, Smith G.L., PhD^{*2}, Mummery
10 C.L., PhD^{*1,7}, Burton F.L., PhD^{*2}

11 # these authors contributed equally to this work

12 * authors for correspondence and equal contributions

13
14
15
16 **Affiliations:**

17 ¹ Dept. of Anatomy and Embryology, Leiden University Medical Center, Einthovenweg 20, 2333 ZD
18 Leiden, The Netherlands.

19 ² Institute of Cardiovascular and Medical Sciences, University of Glasgow, G12 8QQ, Glasgow,
20 United Kingdom.

21 ³ Hubrecht Institute, Uppsalalaan 8, 3584 CT Utrecht, The Netherlands.

22 ⁴ Dept. of Stem Cell Biology, University of Nottingham, University Park, NG7 2RD, Nottingham,
23 United Kingdom.

24 ⁵ Department of Experimental Pharmacology and Toxicology, University Medical Center Hamburg
25 Eppendorf, Martinistraße 52, 20246, Hamburg, Germany.

26 ⁶ Hart Long Centrum, Leiden University Medical Center, Albinusdreef 2, 2333 ZA Leiden, The
27 Netherlands.

28 ⁷ Dept. of Applied Stem Cell Technologies, University of Twente, Drienerlolaan 5, 7522 NB
29 Enschede, The Netherlands.

30
31
32
33
34
35
36 **Short Title: Open software to quantify cardiac contraction**

37
38 **Correspondence to:**

39 **Christine L Mummery**

40 Professor of Developmental Biology

41 Chair Dept. of Anatomy & Embryology

42 Leiden University Medical Center (LUMC)

43 Address: Einthovenweg 20, 2333 ZC Leiden (NL)

44 Postal Zone: S-1-P, P.O. Box 9600 2300 RC Leiden (NL)

45 c.l.mummery@lumc.nl

46
47
48
49 **Total word count: 6,742**

50
51 **Subject codes:** Contraction; Basic science; Arrhythmia; Software tool; Pluripotent Stem Cell derived
52 cardiomyocytes.

Commented [BvM1]: PLEASE DO NOT REMOVE TRACKED
CHANGES. You are welcome to add changes.

Commented [BvM2]: Diogo, please check

Commented [BvM3R2]:

53 Abstract

54 **Rationale:** There are several methods to measure cardiomyocyte (CM) and muscle contraction but
55 these require customized hardware, expensive apparatus and advanced informatics or can only be
56 used in single experimental models. Consequently, data and techniques have been difficult to
57 reproduce across models and laboratories, analysis is time consuming and only specialist researchers
58 can quantify data.

59 **Objective:** Here we describe and validate an automated, open source software tool
60 (MUSCLEMOTION) adaptable for use with standard laboratory- and clinical imaging equipment that
61 enables quantitative analysis of normal cardiac contraction, disease phenotypes and pharmacological
62 responses.

63 **Methods and Results:** MUSCLEMOTION allowed rapid and easy measurement of contractility from
64 high-speed movies in: (i) 1-dimensional *in vitro* models such as isolated adult and human pluripotent
65 stem cell-derived CMs (hPSC-CMs); (ii) 2-dimensional *in vitro* models, such as beating CM
66 monolayers or small clusters of hPSC-CMs; (iii) 3-dimensional multicellular *in vitro* or *in vivo*
67 contractile tissues such as cardiac "organoids", engineered heart tissues (EHT), zebrafish- and human
68 hearts. MUSCLEMOTION was effective under different recording conditions (bright field
69 microscopy with simultaneous patch clamp recording, phase contrast microscopy and traction force
70 microscopy). Outcomes were virtually identical to the current gold standards for contraction
71 measurement such as optical flow, pole deflection, edge-detection systems or manual analyses.
72 Finally, we used the algorithm to quantify contraction in *in vitro* and *in vivo* arrhythmia models and to
73 measure pharmacological responses.

74 **Conclusions:** Using a single open source method for processing video recordings, we obtained
75 reliable pharmacological data and measures of cardiac disease phenotype in experimental cell-,
76 animal- and human models.

77
78

79 Non-standard Abbreviations and Acronyms

80	AP	action potential
81	CM	cardiomyocyte
82	EHT	Engineered Heart Tissue
83	GNB5	G protein β subunit 5
84	HCM	hypertrophic cardiomyopathy
85	hiPSC	human induced pluripotent stem cell
86	ISO	isoprenaline
87	LQT1	Long QT Syndrom Type 1
88	MEA	multi electrode array
89	NIFE	nifedipine
90	PDMS	polydimethylsiloxane
91	SNR	signal-to-noise ratio

92
93
94

95 Introduction

96 The salient feature of cardiomyocytes (CMs) is their ability to undergo cyclic contraction and
97 relaxation, a feature critical for cardiac function. In many research laboratories and clinical settings it
98 is therefore essential that cardiac contraction can be quantified at multiple levels, from single cells to
99 multicellular or intact cardiac tissues. Measurement of contractility is relevant for analysis of disease
100 phenotypes, cardiac safety pharmacology, and longitudinal measures of cardiac function over time,
101 both *in vitro* and *in vivo*. In addition, human genotype-phenotype correlations, investigation of cardiac
102 disease mechanisms and the assessment of cardiotoxicity are increasingly performed on human
103 induced pluripotent stem cells (hiPSCs) derived from patients¹⁻³. Many of these studies are carried out
104 in non-specialist laboratories so that it is important that analysis methods are simplified such that they
105 can be used anywhere with access to just standard imaging equipment. Here, we describe a single

106 method with high versatility that can be applied to most imaging outputs of cardiac contraction likely
107 to be encountered in the laboratory or clinic.
108 Electrical and calcium signals are usually quantified *in vitro* using established technologies such as
109 patch clamp electrophysiology, multi electrode arrays (MEAs), cation-sensitive dyes or cation-
110 sensitive genetic reporters⁴. Although experimental details differ among laboratories, the values for
111 these parameters are with some approximations comparable across laboratories, cardiomyocyte source
112 and cell culture configuration (e.g. single cells, multicellular 2-Dimensional (2D) CM monolayers, 3-
113 Dimensional (3D) cultures)^{5,6}. However, there is no comparable method for measuring cardiac
114 contraction across multiple platforms, despite this being a crucial functional parameter affected by
115 many diseases or drugs⁷. We have developed a method to address this that is built on existing
116 algorithms and is fully automated, but most importantly can be used on videos, image stacks or image
117 sequences loaded in the open source image processing program ImageJ⁸. Moreover, it is an open
118 source, dynamic platform that can be expanded, improved and integrated for customized applications.
119 The method, called MUSCLEMOTION, determines dynamic changes in pixel intensity between
120 image frames and expresses the output as a relative measure of [displacement-contraction](#) during
121 muscle contraction and relaxation. We applied the concept to a range of biomedical- and
122 pharmacologically relevant experimental models that included single hPSC-CMs, patterned- or 2D
123 cultures of hPSC-CMs, cardiac organoids, engineered heart tissues (EHTs) and isolated adult rabbit
124 CMs. Results were validated by comparing outputs of the tool with those from three established
125 methods for measuring contraction: optical flow, post deflection and fractional shortening of
126 sarcomere length. These methods have been tailored to (or only work on) specific cell configurations.
127 Traction force microscopy, fractional shortening of sarcomere length and microposts are
128 predominantly suitable for single cells^{8,9}. Cardiomyocyte edge or perimeter detection is suitable for
129 adult CMs but challenging for immature hPSC-CMs due to poorly defined plasma membrane borders
130 and concentric contraction¹⁰, while large post deflection is suitable for EHTs or small cardiac
131 bundles¹¹ but less so for single cells. Our MUSCLEMOTION software by contrast can be used for all
132 of these applications without significant adaptations. Furthermore, it can be used for multi-parameter
133 recording conditions and experimental settings using transmitted light microscopy, fluorescent
134 membrane labeling, fluorescent beads embedded in soft substrates or patch clamp video recordings.
135 Drug responses to positive and negative inotropic agents were evaluated across four different
136 laboratories in multiple cell configurations using MUSCLEMOTION with reliable predictions of drug
137 effects from all laboratories. Furthermore, MUSCLEMOTION was also applicable to optical
138 recordings of zebrafish hearts *in vivo*, where it represented a significant time-saving in analysis, and in
139 human echocardiograms. This versatile tool thus provides a rapid and straightforward way to detect
140 disease phenotypes and pharmacological responses *in vitro* and *in vivo*.

141
142

143 **Methods**

144 Extended methods are in the Online Supplements. The datasets generated and/or analyzed during the
145 current study are available from the corresponding authors on reasonable request.

146 **Code Availability**

147 MUSCLEMOTION source code [has been written in the ImageJ Macro Language](#) and is included in
148 the Online Supplements and is available for use and further development.

149 **Model Cell**

150 The *in silico* cardiomyocyte-like model (Fig. 1d,f,g) was created using Blender v2.77.

151 **Optical Flow analysis**

152 Optical flow analysis was implemented in LabVIEW as described by Hayakawa et al.^{12,13}.

153 **Generation of hiPSC-HCM isogenic triplet using CRISPR/Cas9**

154 [Heterozygous and homozygous mutations were introduced in the ReBL-PAT hiPSC line.](#)

155 **hPSC Culture and Differentiation**

156 hPSCs from multiple independent cell lines (Table S1) were differentiated to CMs as previously
157 described¹⁴⁻¹⁷, or with the Pluricyte® Cardiomyocyte Differentiation Kit (Pluriomics b.v.) according
158 to the manufacturer's protocol. Experiments were performed at 18-30 days after initiation of

Commented [BvM4]: Chris, Diogo, could you please provide details and a reference for the ReBL-PAT line here.

159 differentiation, depending on the cell source and configuration. Pluricytes® were kindly provided by
160 Plurionics b.v.

161 **Patch Clamp Recordings on hPSC-CMs**

162 Electrophysiological recordings of isolated hPSC-CMs were performed as previously described¹⁶.

163 [MEA Recordings on hPSC-CMs](#)

164 [Field potentials from MEAs were recorded and analyzed as previously published](#) ¹⁸.

165 **Movement of embedded beads**

166 Gelatin-patterned polyacrylamide gels containing fluorescent beads were generated and analyzed as
167 described previously¹⁹.

168 **Monolayers of hPSC-CMs**

169 25k-40k cells were plated per Matrigel-coated glass ø10 mm coverslip.

170 **Cardiac Organoids**

171 Cardiac organoids composed of hPSC-CMs and hPSC-derived endothelial cells, were generated as
172 previously described¹⁷.

173 **Adult cardiomyocytes**

174 CMs were isolated from New Zealand White male rabbits as previously described ²⁰.

175 **Membrane labelling**

176 hPSC-CMs were plated on Matrigel-coated glass-bottom 24-well plates and labelled with CellMask
177 Deep Red according to the manufacturer's instructions.

178 **Engineered heart tissues**

179 EHTs were generated and analyzed as previously described¹⁴.

180 **Zebrafish hearts**

181 Zebrafishes hearts were recorded, treated and analysed as previously described ²³.

182 **Echocardiograms**

183 Anonymized ultrasounds of 5 adult patients were selected from the echocardiography database of the
184 Leiden University Medical Center.

185 **Statistics**

186 One-way ANOVA for paired or unpaired measurements was applied to test the differences in means
187 on normalized drug effects. P-values obtained from two-tailed pairwise comparisons were corrected
188 for multiple testing using Bonferroni's method. Statistical analyses were performed with R v3.3.3. P-
189 values lower than 0.05 were considered statistically significant and indicated with an asterisk (*). [N-](#)
190 [values represent biological repeats.](#)

191

192

193 **Results**

194 **Algorithm development**

195 The principle underlying the algorithm of MUSCLEMOTION is the assessment of contraction using
196 an intuitive approach quantifying absolute changes in pixel intensity between a reference frame and
197 the frame of interest, which can be described as

198

199

$$|img_i - img_{ref}| = img_{result}$$

200

201 where img_i is the frame of interest, img_{ref} is the reference frame and img_{result} is the resulting
202 image. For every pixel in the frame, each reference pixel is subtracted from the corresponding pixel of
203 interest and the difference is presented in absolute numbers. Unchanged pixels result in low (black)
204 values, while pixels that are highly changed result in high (white) values (**Fig. 1a**). Next, the mean
205 pixel intensity of the resulting image is measured. This is a quantitative measure of how much the
206 pixels have moved compared to the reference frame: more white pixels indicate more changing pixels
207 and, thus, more displacement. When a series of images is analysed relative to the same reference
208 image, the output describes the accumulated displacement over time (measure of displacement, **Fig.**
209 **1b**).

210 However, if a series of images is analysed with a reference frame that depends on the frame of interest
211 (e.g. $img_{ref} = img_{i-1}$), this results in a measure of the relative displacement per interframe interval.
212 We defined this parameter as contraction velocity (measure of velocity, **Fig. 1b**).

213 Since velocity is the first derivative of displacement in time, the first derivative of the
214 measure of displacement should resemble the measure of velocity derived from image calculations.
215 To test the linearity of the method, three movies of moving blocks were analysed. The block moved
216 back and forth at two different speeds in each direction (where $v_2 = 2 \cdot v_1$): i) along the x-axis, ii)
217 along the y-axis and iii) along both axes (**Movie S1**). As expected, the measure of displacement and
218 velocity showed a linear correlation (**Fig. S1**). This does not hold when the position of the block in
219 img_i does not overlap the position of the block in img_{ref} , with a consequent saturation in the
220 measure of displacement (i.e. max pixel white value, **Fig. S2**). Therefore, comparison of the
221 differentially derived velocities should approximately overlap in the absence of pixel saturation. This
222 was used as a qualitative parameter to determine whether the algorithm outputs were reliable.

223 224 **Algorithm implementation**

225 MUSCLEMOTION was then modified to handle typical experimental recordings by (i) improving the
226 signal-to-noise ratio (SNR), (ii) automating reference frame selection and (iii) programming built-in
227 checks to validate the generated output data (**Fig. 1c**). The SNR was increased by isolating the pixels
228 of interest in a three-step process: i) maximum projection of pixel intensity in the complete
229 ~~displacement-contraction~~ stack, ii) creation of a binary image of this maximum projection with a
230 threshold level equal to the mean grey value plus standard deviation and iii) multiplication of the pixel
231 values in this image by the original ~~contraction-displacement~~ and speed of the ~~contraction~~
232 ~~displacement~~ image stack (**Fig. S3**). This process allowed the algorithm to work on a region of
233 interest with movement above the noise level only.

234 Next, a method was developed to identify the correct img_{ref} from the speed of ~~displacement~~
235 ~~contraction~~ image stack by comparing values obtained from the frame-to-frame calculation with their
236 direct neighbouring values, while also checking for the lowest absolute value (**Fig. S4**).

237 The reliability of MUSCLEMOTION for structures with complex movements was validated using a
238 custom-made contracting 3D “synthetic CM” model (**Fig. 1d,f,g**) that was adapted to produce
239 contractions with known amplitude and duration. Linearity was preserved during the analysis of the
240 contraction and velocity; other output parameters of the analysis matched the input parameters (**Fig.**
241 **1e**). A second 3D model (**Fig. 1g**), with a repetitive pattern aimed to create out-of-bounds problems
242 was also generated. As expected, contraction amplitude information here was not linear (**Fig. 1e**),
243 although contraction velocity and temporal parameters did remain linear (**Fig. 1e,g**). To mitigate this
244 problem, we implemented an option for a 10-sigma Gaussian blur filter that can be applied on demand
245 to biological samples that presented highly repetitive patterns (e.g. sarcomeres in adult CMs).

246 247 248 **Algorithm application to multiple cell configurations and correlation with existing gold** 249 **standards**

250 This set of experiments aimed to investigate the versatility of MUSCLEMOTION and examine how
251 its performance compared with standard measures used in each system: i) optical flow for isolated
252 hPSC-CMs, monolayers and organoids; ii) post deflection for EHT; iii) sarcomere length fractional
253 shortening for adult CMs. Remarkably, standard methods currently used measure only contraction or
254 contraction velocity. Linearity was preserved in all cases during the analyses, demonstrating the
255 reliability of the results (**Fig. S5**).

256 First, single hPSC-CMs (**Fig. 2a, Movie S2**) exhibited concentric contraction (**Fig. 2a ii**) and
257 contraction velocity amplitudes correlated well with the amplitudes obtained by optical flow analysis
258 ($R^2 = 0.916$) (**Fig. 2a v**). In contrast to single cells, the area of ~~displacement-contraction~~ for hPSC-CM
259 monolayers was distributed heterogeneously throughout the whole field (**Fig. 2b ii, Movie S3**).
260 Optical flow analysis was compared with our measure of velocity (**Fig. 2b iv**); this showed a good
261 linear correlation ($R^2 = 0.803$) (**Fig. 2b v**). Complex (mixed, multicellular) 3D configurations were
262 also investigated by analyzing hPSC-derived cardiac organoids¹⁷ (**Movie S4**) and EHTs¹⁴ (**Movie S5**).
263 Cardiac organoids showed moderate levels of ~~displacement-contraction~~ throughout the tissue (**Fig. 2c**
264 **ii**), while the EHTs showed high deflection throughout the bundle (**Fig. 2d ii**). The contraction
265 velocity of the organoids correlated well with the output of optical flow analysis ($R^2 = 0.747$, **Fig. 2c**
266 **v**). Similarly, contraction amplitudes in EHTs showed high linear correlation ($R^2 = 0.88949$) with the

267 absolute force values derived from measurement of pole deflection (**Fig. 2d v**). Finally, single adult
268 rabbit ventricular CMs were analyzed (**Fig. 2e, Movie S6**). Large ~~displacements-movement were was~~
269 evident around the long edges of the CM (**Fig. 2e ii**). These cells were analyzed with a 10-sigma
270 Gaussian blur filter, which also minimized (unwanted) effects of transverse movements on contraction
271 patterns. Linearity was preserved (**Fig. S5**) despite the repetitive pattern of the sarcomeres and this
272 resulted in accurate measures of both contraction (**Fig. 2e iii**) and speed of contraction (**Fig. 2e iv**).
273 The contraction amplitude of the adult CMs stimulated at 1 Hz correlated well with the output of
274 sarcomeric shortening using fast Fourier transform analysis²¹ ($R^2 = 0.871$, **Fig. 2e v**). Thus, the
275 MUSCLEMOTION algorithm yielded data in these initial studies comparable with methods of
276 analysis tailored for the individual platforms.

277 **Application of MUSCLEMOTION to multiple imaging and recording platforms**

278 To examine whether MUSCLEMOTION could potentially be used in applications that measure other
279 aspects of CMs functionality in parallel, we first determined the electrophysiological properties of
280 hPSC-CMs using patch clamp whilst recording their contractile properties through video imaging.
281 This allowed simultaneous quantitative measurement of action potentials (APs) and contraction (**Fig.**
282 **3a**), for in-depth investigation of their interdependence. We observed a typical²² profile of AP
283 followed by its delayed contraction.

284 To measure contractile force in combination with contractile velocity in single CMs, we integrated
285 fluorescent beads into polyacrylamide substrates patterned with gelatin (**Fig. 3b**), where the
286 displacement of the beads is a measure of CM contractile force¹⁹ (**Movie S7**).

287 ~~Field potentials and contraction profiles of hPSC-CMs were analyzed from simultaneous electrical~~
288 ~~and video recordings of monolayers plated on MEAs (Fig 3c, Movie S8).~~

289 Similarly, effective quantification of contraction profiles was obtained for fluorescently labeled
290 hPSC-CM monolayer cultures (**Fig. 3de, Movie S9**), allowing MUSCLEMOTION to be integrated
291 on high speed fluorescent microscope systems for automated data analysis.

293 **Application of MUSCLEMOTION to drug responses in different cell models in different laboratories**

294 Having shown that MUSCLEMOTION was fit-for-purpose in analyzing contraction over a variety of
295 platforms, we next sought to demonstrate its ability to detect the effects of positive and negative
296 inotropes. This is essential for ensuring the scalability of the tool over multiple platforms, particularly
297 in the context of hiPSC-CMs where regulatory authorities and pharmaceutical companies are
298 interested in using these cells as human heart models for drug discovery, target validation or safety
299 pharmacology²³. For isoprenaline (ISO) and nifedipine (NIFE) the main parameters of interest are:
300 contraction amplitude (ISO, NIFE), relaxation time (ISO) and contraction duration (NIFE).
301

302
303 The relaxation time of spontaneously beating isolated hPSC-CMs on gelatin patterned polyacrylamide
304 substrates treated with ISO significantly decreased as expected at doses higher than 1 nM. Similar to
305 what has been reported²⁷, contraction amplitude decreased at doses higher than 1 nM. NIFE treatment
306 decreased both contraction amplitude and duration starting from 3 nM, respectively (**Fig. 4a**). In
307 paced (1.5 Hz) hPSC-CMs monolayers, no significant effects were measured after addition of ISO on
308 either relaxation time or contraction amplitude. NIFE caused a progressive decrease in contraction
309 duration and amplitude in a concentration-dependent manner starting at 100 nM (**Fig. 4b**). Similarly,
310 cardiac organoids paced at 1.5 Hz showed no significant effects on both relaxation time and
311 contraction amplitude with ISO, while both parameters decreased after NIFE, starting from 100 nM
312 and 300 nM, respectively (**Fig. 4c**). EHTs paced at 1.5 times baseline frequency and analyzed with
313 MUSCLEMOTION showed a positive inotropic effect starting from 1 nM ISO and a negative
314 inotropic effect starting at 30 nM NIFE as previously reported¹⁴ (**Fig. 4d**).

315 Paced (1 Hz) adult rabbit CMs exhibited no significant increase in relaxation time and contraction
316 amplitude at any ISO concentration. At concentrations higher than 3 nM, adult CMs exhibited after-
317 contractions and triggered activity during diastole, which hampered their ability to be paced at a fixed
318 frequency. No significant effects were observed on contraction duration with NIFE, while contraction
319 amplitude significantly decreased in a dose-dependent manner starting from 100 nM (**Fig. 4e**). Data
320 generated by post deflection and sarcomere fractional shortening are available for comparison
321 purposes in **Fig. S6**.

Formatted: Font: Bold

Formatted: Font: Not Bold

Analysis of disease phenotypes *in vitro*

Contractility of hiPSC-CMs carrying mutations associated with Long QT Syndrome Type 1 (LQT1) and hypertrophic cardiomyopathy (HCM) were characterized in distinct cell configurations: monolayers plated on MEAs and EHTs, respectively. As demonstrated previously, LQT1 phenotype was captured as a prolongation of the QT interval of the field potential^{16,24}. As expected, contraction duration measured with MUSCLEMOTION was also prolonged (Fig. 5a,b). EHTs were fabricated from an isogenic triplet carrying the MYH7^{R453C} mutation in homozygosis and heterozygosis and showed a gene dosage effect on the contractility recapitulating disease severity.

Analysis of disease phenotypes *in vivo*

To extend analysis to hearts *in vivo*, we took advantage of the transparency of zebrafish, which allows recording of contracting cardiac tissue *in vivo* (Fig. 65a, Movie S109). It was previously shown that mutations in G protein β subunit 5 (*GNB5*) are associated with a multisystem syndrome in human, with severe bradycardia at rest. Zebrafish with loss of function mutations in *gnb5a* and *gnb5b* were generated. Consistent with the syndrome manifestation in patients, zebrafish *gnb5a/gnb5b* double mutant embryos showed severe bradycardia in response to parasympathetic activation²⁵. Irregularities in heart rate were visually evident and were clearly distinguishable from the wild type counterpart after analysis with MUSCLEMOTION (Fig. 65b). Quantification of the heart rate of these zebrafishes with MUSCLEMOTION highly correlated ($R^2 = 0.98$) with the results of the published manual analyses²⁵ (Fig. 65c). There was however, a striking time-saving for operators in carrying out the analysis using the algorithm (5-10 times faster than manual analysis; 150 recordings were analysed in 5 hours versus 4 days) without compromising accuracy of the outcome. Qualitative analysis of contraction patterns allowed rapid discrimination between arrhythmic vs non-arrhythmic responses to carbachol treatment (Fig. 65c).

Finally, we examined human echocardiograms from five healthy and cardiomyopathic individuals (Fig. 65d, Movie S11). To assess ventricular function, videos were cropped to exclude movement contributions of the atria and valves. MUSCLEMOTION enabled rapid quantification of temporal parameters from standard ultrasound echography (Fig. 65e) such as time-to-peak, relaxation time, RR interval and the contraction duration (Fig. 65f).

Discussion

A reliable and easy-to-use method to quantify cardiac muscle contraction would be of significant benefit to many basic and clinical science laboratories to characterize cardiac disease phenotypes, understand underlying disease mechanisms and predicting cardiotoxic effects of drugs^{14,26}. Quantification of frame-to-frame differences in pixel intensity has been used in recent reports with success¹⁰; however, the full spectrum of applications for which these algorithms are relevant, how their output data correlates with gold standards in each system and software performance, specifications, license and software availability, have remained unclear.

Here we developed and tested a user-friendly, inexpensive, open source software platform that serves this purpose in a variety of biological systems of heart tissue. Its integration into current research practices would benefit data sharing, reproducibility, comparison and translation in many clinically relevant contexts²⁷.

The linearity and reliability of MUSCLEMOTION were validated using a 3D reconstructed artificial CM which gave the expected linear correlations between known inputs and the outputs (Fig. 1d-f). When random repetitive patterns were applied, amplitude outputs differed from inputs, suggesting a potential limitation to measuring contraction amplitudes in highly repetitive biological samples (such as when sarcomere patterns are well-organized), while temporal parameters remained valid (Fig. 1d,e,g). However, conditions such as these would be unlikely in standard biological samples, where camera noise significantly reduces the possibility of saturating pixel movement. We partially attenuated this problem by applying, on user demand, a 10-sigma Gaussian blur filter which significantly increased the accuracy of MUSCLEMOTION with highly repetitive structures. Also, to

376 increase reliability, we built in additional controls to detect any mismatches and errors.
377 MUSCLEMOTION can automatically identify and select the reference frame and increase the signal-
378 to-noise-ratio, features which were particularly relevant in reducing user bias and interaction while
379 improving user experience. MUSCLEMOTION is valid in a wide range of illumination conditions
380 without changing temporal parameters; however, exposure time was linearly correlated with
381 contraction amplitude (Fig. S7). [Furthermore, a series of situations where no contraction is present](#)
382 [has been used as a negative control \(Fig. S8\)](#). Batch mode analyses and data storage in custom folders
383 were also incorporated to support overnight automated analyses. For accurate quantification of
384 amplitude, time-to-peak and relaxation time, an appropriate sampling rate should be chosen. For
385 applications similar to those described here, we recommend recording rates higher than 70 frames per
386 second to sample correctly the fast upstroke of the time-to-peak typical of cardiac tissue. This
387 recording rate is easily achievable even using smartphone slow motion video options (~120/240
388 frames per second), obviating the need for dedicated cameras and recording equipment if necessary.
389 We demonstrated excellent linear correlations between our software tool and multiple other standard
390 methods independent of substrate, cell configuration and technology platform and showed that
391 MUSCLEMOTION is able to capture contraction in a wide range of *in vivo* and *in vitro* applications
392 (Fig. 2 and Fig. 3). Specifically, we identified several advantages compared to optical flow algorithms
393 in terms of speed and the absence of arbitrary binning factors or thresholds which, when modified,
394 profoundly affect the results. One limitation compared to optical flow or EHT standard algorithm is
395 that the tool lacks qualitative vector orientation, making it more difficult to assess contraction
396 direction. Particularly important was the correlation with force data calculated from the displacement
397 of flexible posts by EHTs. This indicates that when the mechanical properties of substrates are
398 known²⁸, MUSCLEMOTION allows absolute quantification of contractile force. Technical limitations
399 of the EHT recording system allowed us to analyze only movies with JPEG compression; this resulted
400 in loss of pixel information that might have negatively influenced the correlation shown. For better
401 and more accurate results on contraction quantification, non-lossy/uncompressed video formats
402 should be used for recordings since individual pixel information is lost upon compression and
403 therefore not available for analysis by MUSCLEMOTION.
404 We proposed and validated practical application in pharmacological challenges using multiple
405 biological preparations recorded in different laboratories; this means that immediate use in multiple
406 independent high-throughput drug-screening pipelines is possible without further software
407 development being required, as recently applied for a drug screening protocol on cardiac organoids
408 from hPSCs¹⁷. Intuitively, the possibility of having inter-assay comparisons will also be of particular
409 relevance where comparisons of contraction data across multiple platforms are required by regulatory
410 agencies or consortia (e.g. CiPA, CSAHi)^{5,6,23,29}. Moreover, this might offer a quantitative approach to
411 investigating how genetic or acquired diseases of the heart (e.g. cardiomyopathies⁷, Long QT
412 Syndrome³⁰), heart failure resulting from anticancer treatments^{31,32} or maturation strategies^{19,33,34}
413 affect cardiac contraction. The possibility of linking *in vitro* with *in vivo* assays, with low cost
414 technologies applicable with existing hardware certainly represents an advantage as demonstrated by
415 automatic quantification of zebrafish heartbeats and human echocardiograms (Fig. 6S). Overall, these
416 results clearly demonstrated that contraction profiles could be derived and quantified in a wide variety
417 of commonly used experimental and clinical settings. MUSCLEMOTION might represent a starting
418 point for a swift screening method to provide clinically relevant insights into regions of limited
419 contractility in the hearts of patients. We encourage further development of this open source platform
420 to fit specific needs; future areas of application could include skeletal or smooth muscle in the same
421 range of formats described here.
422 MUSCLEMOTION allows the use of a single, transparent method of analysis of cardiac contraction
423 in many modalities for rapid and reliable identification of disease phenotypes, potential cardiotoxic
424 effects in drug screening pipelines and translational comparison of contractile behaviour.

425
426

427 Limitations

428 Saturation of pixel movements may affect contraction amplitudes. However, as demonstrated with the
429 artificial CM, contraction velocity and all temporal parameters remained valid. We also minimized the

430 impact of highly repetitive structures on the output of MUSCLEMOTION by applying a Gaussian
431 filter, which also helped in reducing the impact of transverse movements on contraction profiles. High
432 frequency contraction might complicate baseline detection, especially if the duration of the contracted
433 state is similar to that of the relaxed (e.g. approaching sinusoidal). We have implemented a “fast
434 mode” option that captures reliable baseline values even at high contraction rates. Furthermore,
435 recordings must be free of moving objects (e.g. debris moved by flow, air bubbles) other than those of
436 interest. [MUSCLEMOTION does not measure absolute values of cell shortening or force of
437 contraction. However, as demonstrated by correlations with these physical quantities \(Fig. 2d,e v\) ,
438 specific setups can be calibrated to obtain such readout.](#)
439 [Adult CMs contract dominantly along the longitudinal axis. However, hPSC-CMs highly vary in
440 shape, often showing concentric contractions, effects of transverse movement are usually intrinsic to
441 the experimental model and should be considered in the global contraction analysis. Indirect
442 transverse movements originating from uncontrolled experimental conditions \(e.g. sample shift,
443 floating debris, etc.\) should be avoided since it might introduce an overestimation of the
444 cardiomyocyte contraction.](#)

445
446

447 Sources of Funding

448 This work was initiated in the context of The National Centre for the Replacement, Refinement and
449 Reduction of Animals in Research (NC3Rs) CRACK IT InPulse project code 35911-259146, with
450 support from GlaxoSmithKline. It was supported by the following grants: ERC-AdG
451 STEMCARDIOVASC (MCL MBJ, GE, BM, TLGJ), ZonMW MKMD *Applications of Innovations*
452 *2015-2016* (MCL, BM, SL), BHF SP/15/9/31605 & PG/14/59/31000 and BIRAX 04BX14CDLG
453 grants (DC), ERC-AdG IndivHeart (ET) and DZHK (German Centre for Cardiovascular Research;
454 ET, SU, HA, MI), ERC-StG StemCardioRisk (DRP, MPMH), VIDI-917.15.303 (the Netherlands
455 Organisation for Scientific Research (NWO); DRP, GC). The Dutch Heart Foundation (CVON 2012 –
456 10 Predict project), E-Rare (CoHeart project).

457
458

459 Disclosures

460 MCL and PR are co-founders of Pluriomics B.V.
461 SGL and BF are co-founders of Clyde Biosciences Ltd.
462 ET, HA and MI are co-founders of EHT Technologies GmbH

463
464

465 References

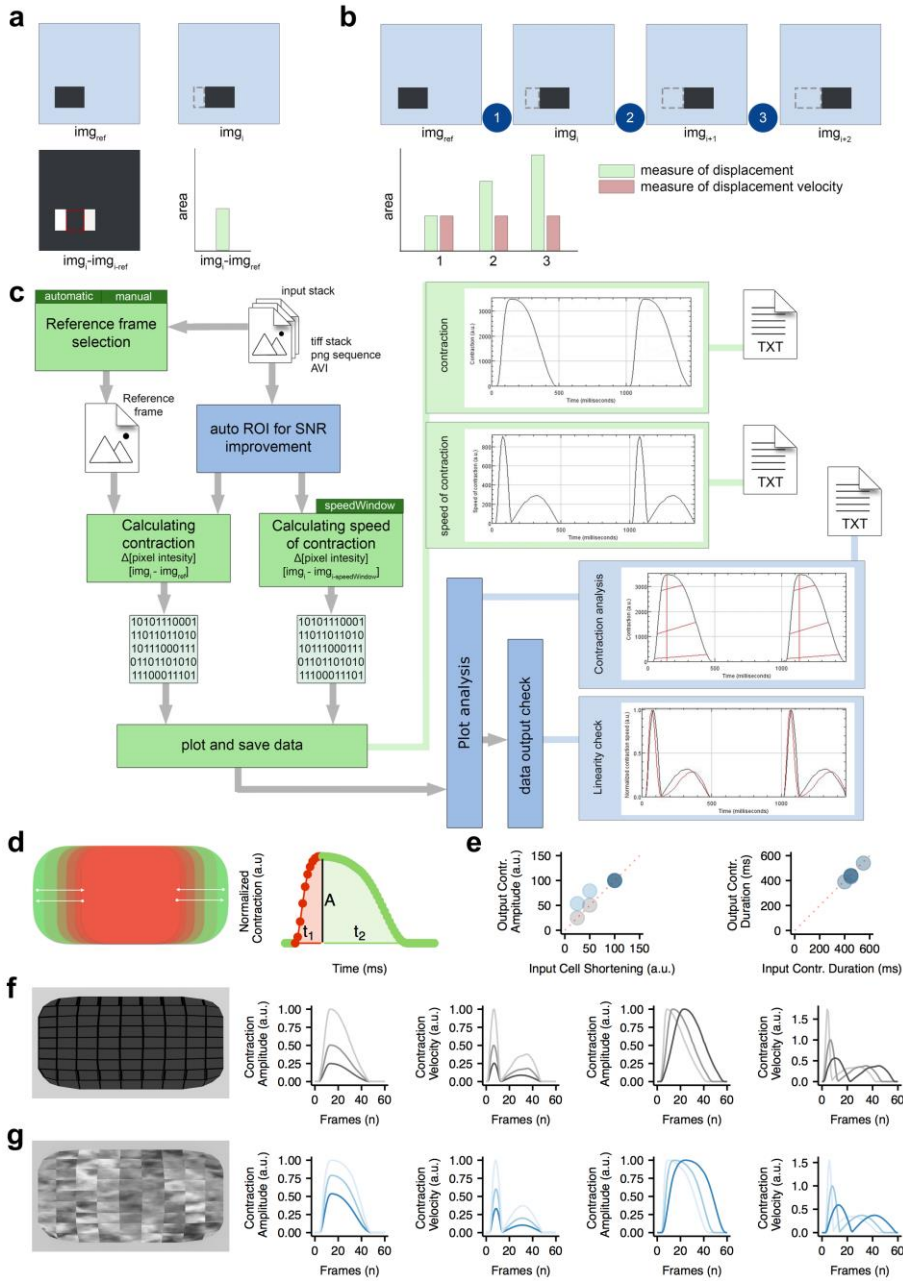
- 466 1. Lavery H, Benson C, Cartwright E, et al. How can we improve our understanding of
467 cardiovascular safety liabilities to develop safer medicines? *Br J Pharmacol.* 2011;163:675–
468 693.
- 469 2. Passier R, Orlova V, Mummery C. Complex Tissue and Disease Modeling using hiPSCs. *Cell*
470 *Stem Cell.* 2016;18:309–321.
- 471 3. Bellin M, Marchetto MC, Gage FH, Mummery CL. Induced pluripotent stem cells: the new
472 patient? *Nat Rev Mol Cell Biol.* 2012;13:713–726.
- 473 4. van Meer BJ, Tertoolen LGJ, Mummery CL. Concise Review: Measuring Physiological
474 Responses of Human Pluripotent Stem Cell Derived Cardiomyocytes to Drugs and Disease.
475 *Stem Cells.* 2016;34:2008–2015.
- 476 5. Kitaguchi T, Moriyama Y, Taniguchi T, et al. CSAHi study: Evaluation of multi-electrode
477 array in combination with human iPS cell-derived cardiomyocytes to predict drug-induced QT
478 prolongation and arrhythmia - Effects of 7 reference compounds at 10 facilities. *J Pharmacol*
479 *Toxicol Methods.* 2016;78:93–102.

- 480 6. Hwang HS, Kryshstal DO, Feaster TK, Sanchez-Freire V, Zhang J, Kamp TJ, Hong CC, Wu
481 JC, Knollmann BC. Comparable calcium handling of human iPSC-derived cardiomyocytes
482 generated by multiple laboratories. *J Mol Cell Cardiol.* 2015;85:79–88.
- 483 7. Birket MJ, Ribeiro MC, Kosmidis G, Ward D, Leitoguinho AR, van de Pol V, Dambrot C,
484 Devalla HD, Davis RP, Mastroberardino PG, Atsma DE, Passier R, Mummery CL. Contractile
485 Defect Caused by Mutation in MYBPC3 Revealed under Conditions Optimized for Human
486 PSC-Cardiomyocyte Function. *Cell Rep.* 2015;13:733–745.
- 487 8. Ribeiro AJS, Ang Y-S, Fu J-D, Rivas RN, Mohamed TMA, Higgs GC, Srivastava D, Pruitt
488 BL. Contractility of single cardiomyocytes differentiated from pluripotent stem cells depends
489 on physiological shape and substrate stiffness. *Proc Natl Acad Sci USA.* 2015;112:12705–
490 12710.
- 491 9. Ribeiro AJS, Schwab O, Mandegar MA, Ang Y-S, Conklin BR, Srivastava D, Pruitt BL.
492 Multi-Imaging Method to Assay the Contractile Mechanical Output of Micropatterned Human
493 iPSC-Derived Cardiac Myocytes. *Circ Res.* 2017;120:1572–1583.
- 494 10. Kijlstra JD, Hu D, Mittal N, Kausel E, van der Meer P, Garakani A, Domian IJ. Integrated
495 Analysis of Contractile Kinetics, Force Generation, and Electrical Activity in Single Human
496 Stem Cell-Derived Cardiomyocytes. *Stem Cell Reports.* 2015;5:1226–1238.
- 497 11. Stoehr A, Neuber C, Baldauf C, et al. Automated analysis of contractile force and Ca²⁺
498 transients in engineered heart tissue. *Am J Physiol Heart Circ Physiol.* 2014;306:H1353–63.
- 499 12. Hayakawa T, Kunihiro T, Ando T, Kobayashi S, Matsui E, Yada H, Kanda Y, Kurokawa J,
500 Furukawa T. Image-based evaluation of contraction–relaxation kinetics of human-induced
501 pluripotent stem cell-derived cardiomyocytes: Correlation and complementarity with
502 extracellular electrophysiology. *J Mol Cell Cardiol.* 2014;77:178–191.
- 503 13. Hayakawa T, Kunihiro T, Dowaki S, Uno H, Matsui E, Uchida M, Kobayashi S, Yasuda A,
504 Shimizu T, Okano T. Noninvasive evaluation of contractile behavior of cardiomyocyte
505 monolayers based on motion vector analysis. *Tissue Eng Part C Methods* [Internet].
506 2012;18:21–32.
- 507 14. Mannhardt I, Breckwoldt K, Letuffe-Brenière D, et al. Human Engineered Heart Tissue:
508 Analysis of Contractile Force. *Stem Cell Reports.* 2016;7:29–42.
- 509 15. van den Berg CW, Elliott DA, Braam SR, Mummery CL, Davis RP. Differentiation of Human
510 Pluripotent Stem Cells to Cardiomyocytes Under Defined Conditions. *Methods Mol Biol.*
511 2016;1353:163–180.
- 512 16. Sala L, Yu Z, Ward-van Oostwaard D, van Veldhoven JP, Moretti A, Laugwitz K-L,
513 Mummery CL, Ijzerman AP, Bellin M. A new hERG allosteric modulator rescues genetic and
514 drug-induced long-QT syndrome phenotypes in cardiomyocytes from isogenic pairs of patient
515 induced pluripotent stem cells. *EMBO Mol Med.* 2016;8:1065–1081.
- 516 17. Giacomelli E, Bellin M, Sala L, van Meer BJ, Tertoolen LGJ, Orlova VV, Mummery CL.
517 Three-dimensional cardiac microtissues composed of cardiomyocytes and endothelial cells co-
518 differentiated from human pluripotent stem cells. *Development.* 2017;144:dev.143438–1017.
- 519 18. Sala L, Ward-van Oostwaard D, Tertoolen LGJ, Mummery CL, Bellin M. Electrophysiological
520 Analysis of human Pluripotent Stem Cell-derived Cardiomyocytes (hPSC-CMs) Using Multi-
521 electrode Arrays (MEAs). *J Vis Exp.* 2017;

- 522 19. Ribeiro MC, Tertoolen LG, Guadix JA, Bellin M, Kosmidis G, D'Aniello C, Monshouwer-
523 Kloots J, Goumans M-J, Wang Y-L, Feinberg AW, Mummery CL, Passier R. Functional
524 maturation of human pluripotent stem cell derived cardiomyocytes in vitro--correlation
525 between contraction force and electrophysiology. *Biomaterials*. 2015;51:138–150.
- 526 20. MacQuaide N, Ramay HR, Sobie EA, Smith GL. Differential sensitivity of Ca²⁺ wave and
527 Ca²⁺ spark events to ruthenium red in isolated permeabilised rabbit cardiomyocytes. *J Physiol*
528 (*Lond*). 2010;588:4731–4742.
- 529 21. Rocchetti M, Sala L, Rizzetto R, et al. Ranolazine prevents INaL enhancement and blunts
530 myocardial remodelling in a model of pulmonary hypertension. *Cardiovasc Res*. 2014;104:37–
531 48.
- 532 22. Bers DM. Cardiac excitation-contraction coupling. *Nature*. 2002;415:198–205.
- 533 23. Sala L, Bellin M, Mummery CL. Integrating cardiomyocytes from human pluripotent stem
534 cells in safety pharmacology: has the time come? *Br J Pharmacol*. 2016;97:2684.
- 535 24. Zhang M, D'Aniello C, Verkerk AO, et al. Recessive cardiac phenotypes in induced
536 pluripotent stem cell models of Jervell and Lange-Nielsen syndrome: disease mechanisms and
537 pharmacological rescue. *Proc Natl Acad Sci USA*. 2014;111:E5383–92.
- 538 25. Lodder EM, De Nittis P, Koopman CD, et al. GNB5 Mutations Cause an Autosomal-
539 Recessive Multisystem Syndrome with Sinus Bradycardia and Cognitive Disability. *Am J Hum*
540 *Genet*. 2016;99:704–710.
- 541 26. Rodriguez ML, Graham BT, Pabon LM, Han SJ, Murry CE, Sniadecki NJ. Measuring the
542 contractile forces of human induced pluripotent stem cell-derived cardiomyocytes with arrays
543 of microposts. *J Biomech Eng*. 2014;136:051005.
- 544 27. Bullen A. Microscopic imaging techniques for drug discovery. *Nat Rev Drug Discov*.
545 2008;7:54–67.
- 546 28. Vandeburgh H, Shansky J, Benesch-Lee F, Barbata V, Reid J, Thorrez L, Valentini R,
547 Crawford G. Drug-screening platform based on the contractility of tissue-engineered muscle.
548 *Muscle Nerve*. 2008;37:438–447.
- 549 29. Cavero I, Holzgreffe H. Comprehensive in vitro Proarrhythmia Assay, a novel in vitro/in silico
550 paradigm to detect ventricular proarrhythmic liability: a visionary 21st century initiative.
551 *Expert Opin Drug Saf*. 2014;13:745–758.
- 552 30. Rocchetti M, Sala L, Dreizehnter L, et al. Elucidating arrhythmogenic mechanisms of long-QT
553 syndrome CALM1-F142L mutation in patient-specific induced pluripotent stem cell-derived
554 cardiomyocytes. *Cardiovasc Res*. 2017;113:531–541.
- 555 31. Burridge PW, Li YF, Matsa E, et al. Human induced pluripotent stem cell-derived
556 cardiomyocytes recapitulate the predilection of breast cancer patients to doxorubicin-induced
557 cardiotoxicity. *Nat Med*. 2016;22:547–556.
- 558 32. Bellin M, Mummery CL. Stem cells: The cancer's gone, but did chemotherapy damage your
559 heart? *Nat Rev Cardiol*. 2016;13:383–384.
- 560 33. Nunes SS, Miklas JW, Liu J, et al. Biowire: a platform for maturation of human pluripotent
561 stem cell-derived cardiomyocytes. *Nat Meth*. 2013;10:781–787.

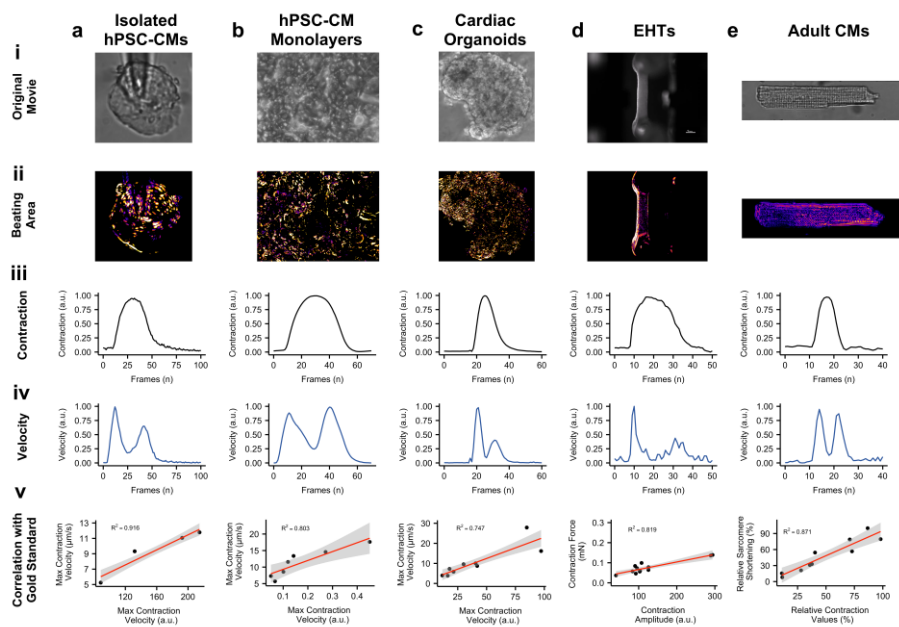
562 34. Chan Y-C, Ting S, Lee Y-K, Ng K-M, Zhang J, Chen Z, Siu C-W, Oh SKW, Tse H-F.
563 Electrical stimulation promotes maturation of cardiomyocytes derived from human embryonic
564 stem cells. *J Cardiovasc Transl Res.* 2013;6:989–999.

565



567
568

569 **Figure 1**
570 **Algorithm construction and validation.**
571 **a)** Principle of pixel intensity difference by subtraction of img_{ref} of img_i and measurement of the non-
572 zero area after image subtraction.
573 **b)** Principle of using pixel intensity difference as a measure of displacement and as a measure of
574 [displacement](#) velocity.
575 **c)** Schematic overview of MUSCLEMOTION. Green blocks indicate basic steps of the algorithm.
576 Dark green blocks indicate important user input choices. Plots within light green blocks indicate
577 results. Optional steps are shown in blue blocks, with graphical representation of the analysed
578 parameters indicated by red lines. Three result files are generated containing the raw data:
579 “contraction.txt”, “speed-of-contraction.txt” and “overview-results.txt”. Furthermore, three images
580 showing relevant traces and a log file are generated and saved (not shown in schematic).
581 **d)** Schematic of the contractile pattern of the artificial cell and relative parameters corresponding to
582 amplitude of contraction (A), time-to-peak (t_1) and relaxation time (t_2).
583 **e)** Correlation between input (x axis) and output (y axis) parameters used to validate
584 MUSCLEMOTION with two artificial cells.
585 **f-g)** Frame representing the two artificial cells built for MUSCLEMOTION validation and their
586 relative output parameters.



587
588

589

Figure 2

Correlation of results with gold standards.

591 **a)** Brightfield image of isolated hPSC-CMs (**i**), with maximum projection step visually enhanced with
592 a fire Look Up Table (**ii**), contraction (**iii**) and velocity (**iv**) profiles of each individual beat have been
593 generated by MUSCLEMOTION and temporally aligned; linear regression analysis between
594 MUSCLEMOTION results (x-axis) and optical flow results (y-axis) (**v**).

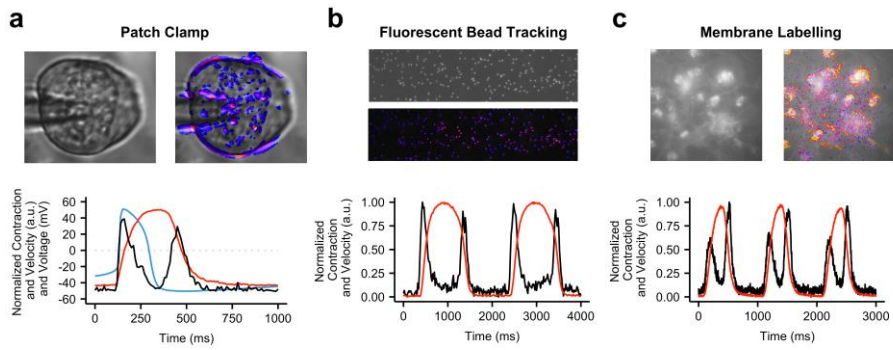
595 **b)** Phase contrast image of hPSC-CM monolayers (**i**), with maximum projection step visually
596 enhanced with a fire Look Up Table (**ii**), contraction (**iii**) and velocity (**iv**) profiles of each individual
597 beat have been generated by MUSCLEMOTION and temporally aligned; linear regression analysis
598 between MUSCLEMOTION results (x-axis) and those obtained with optical flow results (y-axis) (**v**).

599 **c)** Phase contrast image of cardiac organoids (**i**), with maximum projection step visually enhanced
600 with a fire Look Up Table (**ii**), contraction (**iii**) and velocity (**iv**) profiles of each individual beat have
601 been generated by MUSCLEMOTION and temporally aligned; linear regression analysis between
602 MUSCLEMOTION results (x-axis) and those obtained with optical flow results (y-axis) (**v**).

603 **d)** Live view of an EHT during contraction analysis. Scale bar = 1 mm. (**i**), with maximum projection
604 step visually enhanced with a fire Look Up Table (**ii**), contraction (**iii**) and velocity (**iv**) profiles of
605 each individual beat have been generated by MUSCLEMOTION and temporally aligned; linear
606 regression analysis between MUSCLEMOTION results (x-axis) and those obtained with post
607 deflection (y-axis) (**v**).

608 **e)** Brightfield image of adult rabbit CMs (**i**), with maximum projection step visually enhanced with a
609 fire Look Up Table (**ii**); contraction (**iii**) and velocity (**iv**) profiles of each individual beat have been
610 generated by MUSCLEMOTION and temporally aligned; linear regression analysis between
611 MUSCLEMOTION results (x-axis) and those obtained from sarcomere fractional shortening
612 calculation with Fast Fourier Transform (y-axis) (**v**).

613 For details on cell sources and cell lines please refer to the Supplementary Table 1.



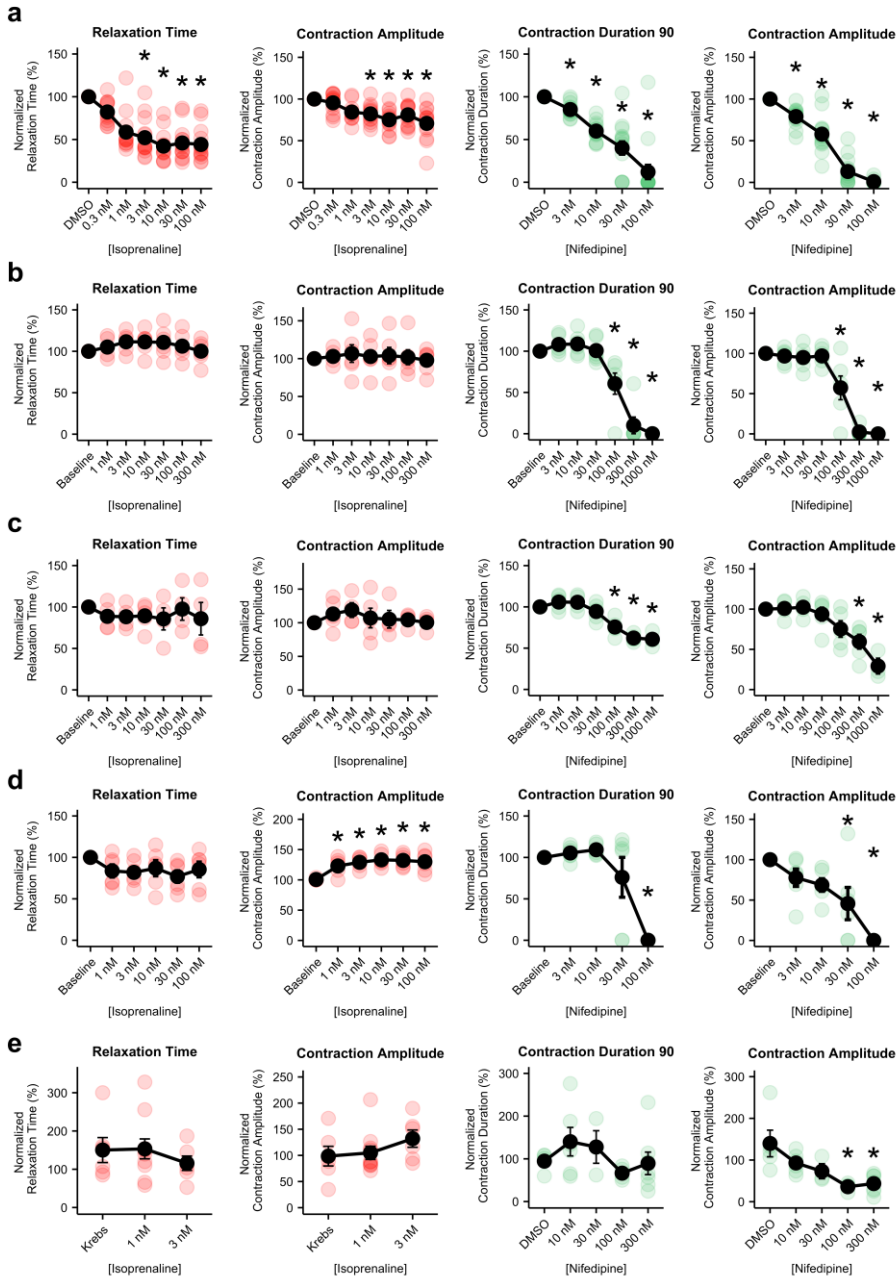
614
615

616

Figure 3

Application of contraction tool to multiple biological situations.

617 Representative examples with enhancement of moving pixels (**top**) and profiles (**bottom**) of
 618 contraction (**a-c, red**), velocity (**a-c, black**) and voltage (**a, blue**) respectively obtained from high
 619 speed movies of patched hPSC-CMs (**a**), aligned hPSC-CMs on polyacrylamide gels with fluorescent
 620 beads (**b**) and hPSC-CMs whose membranes have been labelled with CellMask Deep Red (**c**).
 621
 622 For details on cell sources and cell lines please refer to the Supplementary Table 1.



623
 624 **Figure 4**
 625 **Pharmacological challenge with positive and negative inotropic compounds.**

626 a) Average dose-response curves (**black traces**) and single measurements for several parameters
627 obtained in isolated, spontaneously beating, aligned hPSC-CMs treated with isoprenaline (**left, red**)
628 and nifedipine (**right, green**).

629 b) Average dose-response curves (**black traces**) and single measurements for several parameters
630 obtained from monolayers of hPSC-CMs treated with isoprenaline (**left, red**) and nifedipine (**right,**
631 **green**).

632 c) Average dose-response curves (**black traces**) and single measurements for several parameters
633 obtained in cardiac organoids treated with isoprenaline (**left, red**) and nifedipine (**right, green**).

634 d) Average dose-response curves (**black traces**) and single measurements for several parameters
635 obtained in EHTs treated with isoprenaline (**left, red**) and nifedipine (**right, green**).

636 e) Average dose-response curves (**black traces**) and single measurements for several parameters
637 obtained in adult rabbit CMs treated with isoprenaline (**left, red**) and verapamil (**right, green**).

638 Average data points (**black**) represent mean \pm standard error of mean. For details on cell sources and
639 cell lines please refer to the Supplementary Table 1.

640 Data information: P-values DMSO versus dose. Panel a i) **0.3 nM**: 0.2897; **1 nM**: $3.4 \cdot 10^{-6}$; **3 nM**:
641 $3.8 \cdot 10^{-8}$; **10 nM**: $7 \cdot 10^{-11}$; **30 nM**: $7.3 \cdot 10^{-10}$; **100 nM**: $2.4 \cdot 10^{-10}$. Panel a ii) **0.3 nM**: 1; **1 nM**: 0.0645; **3**
642 **nM**: 0.0136; **10 nM**: $8.2 \cdot 10^{-3}$; **30 nM**: 0.0063; **100 nM**: $2.4 \cdot 10^{-6}$. (N=14; 14; 14; 14; 14; 14)
643 Panel a iii) **3 nM**: 0.6533; **10 nM**: $4 \cdot 10^{-5}$; **30 nM**: $2 \cdot 10^{-9}$; **100 nM**: $1.5 \cdot 10^{-15}$. Panel a iv) **3 nM**:
644 0.00054; **10 nM**: $1.9 \cdot 10^{-11}$; **30 nM**: $< 2 \cdot 10^{-16}$; **100 nM**: $< 2 \cdot 10^{-16}$. (N=14; 14; 14; 14; 14)

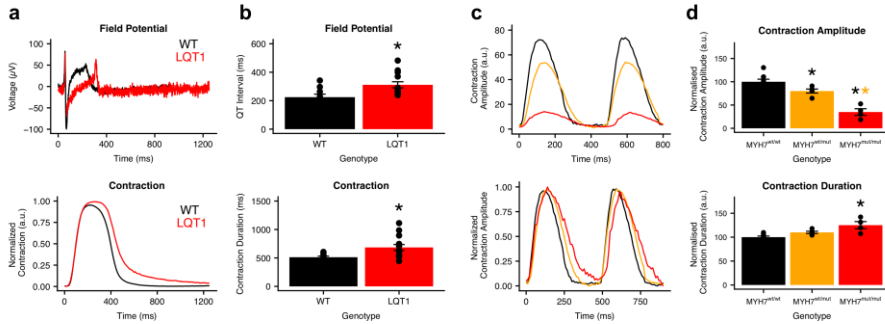
645 P-values baseline versus dose. Panel b i) **1 nM**: 1; **3 nM**: 1; **10 nM**: 1; **30 nM**: 1; **100 nM**: 1; **300 nM**:
646 1. Panel b ii) **1 nM**: 1; **3 nM**: 1; **10 nM**: 1; **30 nM**: 1; **100 nM**: 1; **300 nM**: 1. (N=6; 5; 6; 6; 6; 6)
647 Panel b iii) **3 nM**: 1; **10 nM**: 1; **30 nM**: 1; **100 nM**: 0.00801; **300 nM**: $2.7 \cdot 10^{-9}$; **1000 nM**: $1.8 \cdot 10^{-10}$.
648 Panel b iv) **3 nM**: 1; **10 nM**: 1; **30 nM**: 1; **100 nM**: 0.00084; **300 nM**: $2.9 \cdot 10^{-11}$; **1000 nM**: $1.5 \cdot 10^{-11}$.
649 (N=6; 6; 6; 6; 6; 6)

650 P-values baseline versus dose. Panel c i) **1 nM**: 1; **3 nM**: 1; **10 nM**: 1; **30 nM**: 1; **100 nM**: 1; **300 nM**:
651 1. Panel c ii) **1 nM**: 1; **3 nM**: 1; **10 nM**: 1; **30 nM**: 1; **100 nM**: 1; **300 nM**: 1. (N=5; 5; 4; 5; 4; 4)
652 Panel c iii) **3 nM**: 1; **10 nM**: 1; **30 nM**: 1; **100 nM**: 0.00181; **300 nM**: $2.9 \cdot 10^{-6}$; **1000 nM**: $1.7 \cdot 10^{-5}$.
653 Panel c iv) **3 nM**: 1; **10 nM**: 1; **30 nM**: 1; **100 nM**: 0.54836; **300 nM**: 0.01392; **1000 nM**: $8.2 \cdot 10^{-5}$.
654 (N=5; 5; 4; 5; 5; 3)

655 P-values baseline versus dose. Panel d i) **1 nM**: 1; **3 nM**: 1; **10 nM**: 1; **30 nM**: 0.47; **100 nM**: 1. Panel
656 d ii) **1 nM**: 0.02318; **3 nM**: 0.00170; **10 nM**: 0.00028; **30 nM**: 0.00044; **100 nM**: 0.00113. (N=5; 5;
657 5; 5; 5; 5). Panel d iii) **3 nM**: 1; **10 nM**: 1; **30 nM**: 1; **100 nM**: $3 \cdot 10^{-5}$. Panel d iv) **3 nM**: 1; **10 nM**:
658 0.49856; **30 nM**: 0.01473; **100 nM**: $7 \cdot 10^{-6}$. (N=6; 6; 6; 6; 6)

659 P-values Krebs versus dose. Panel e i) **1 nM**: 1; **3 nM**: 1. Panel e ii) **1 nM**: 1; **3 nM**: 0.54. (N=6; 10;
660 7)

661 P-values DMSO versus dose. Panel e iii) **10 nM**: 1; **30 nM**: 1; **100 nM**: 1; **300 nM**: 1. Panel e iv) **10**
662 **nM**: 0.5298; **30 nM**: 0.2470; **100 nM**: 0.0054; **300 nM**: 0.0029. (N=7; 8; 4; 5; 7).



663
664
665
666
667
668
669
670
671
672
673
674
675

Figure 5

***In vitro* disease phenotypes.**

a) Field potential and contraction profile of wildtype (black) and LQT1 (red) hPSC-CM monolayers on MEAs. **b)** Quantitative analysis of the QT interval and the contraction duration. **c)** Raw (top) and normalized (bottom) contraction profiles of HCM-EHTs. P-values QT-interval: **WT versus LQT1: 0.012**. P-values contraction duration: **WT versus LQT1: 0.012**. **d)** Quantitative analysis of contraction amplitude and contraction duration. P-values contraction amplitude: **MYH7^{wt/wt} versus MYH7^{wt/mt}: 0.026; MYH7^{wt/wt} versus MYH7^{mt/mt}: 6·10⁻⁶; MYH7^{wt/mt} versus MYH7^{mt/mt}: 0.00065**. P-values contraction duration: **MYH7^{wt/wt} versus MYH7^{wt/mt}: 0.062; MYH7^{wt/wt} versus MYH7^{mt/mt}: 0.00085; MYH7^{wt/mt} versus MYH7^{mt/mt}: 0.0046**.

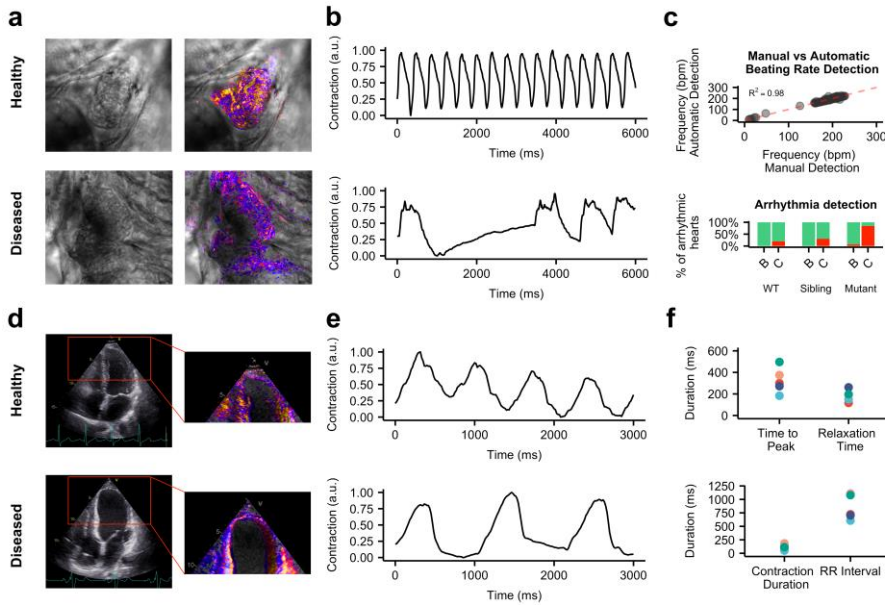
Formatted: Font: (Default) Times New Roman, Bold, Italic

Formatted: Font: Bold

Formatted: Font: Bold

Formatted: Font: Not Bold

676



677

678

679

Figure 65

***In vivo* disease phenotypes.**

680 **a)** Representative examples of wild type (**top**) and *gnb5a/gnb5b* mutant (**bottom**) zebrafishes and
 681 relative enhancement of moving pixels.
 682 **b)** Representative qualitative analyses of normal (**top**) and arrhythmic (**bottom**) contraction profiles
 683 from wild type and *gnb5a/gnb5b* mutant zebrafishes treated with carbachol.
 684 **c)** Correlation of results obtained from manual (x-axis) vs automatic (y-axis) detection of beating
 685 frequency (**top**); distribution of normal (green) and arrhythmic (red) contraction patterns in baseline
 686 frequency (**top**); distribution of normal (green) and arrhythmic (red) contraction patterns in baseline
 687 condition (B) and after treatment with carbachol (C) in wild type and *gnb5a/gnb5b* mutant zebrafishes
 688 (**bottom**).
 689 **d)** Representative echocardiograms of healthy (**top**) and cardiomyopathic (**bottom**) human
 690 individuals. Ventricles have been manually cropped and the enhancement of moving pixels is
 691 overlaid.
 692 **e)** Representative qualitative analyses of normal (**top**) and poor (**bottom**) ventricular functions.
 693 **f)** Quantitative data collected from echocardiogram in 5 individuals. Each colour represents one
 694 individual.